

Determining the Quantum Numbers of Simplified Models in $t\bar{t}X$ production at the LHC

Matthew J. Dolan,¹ Michael Spannowsky,² Qi Wang,² and Zhao-Huan Yu¹

¹*ARC Centre of Excellence for Particle Physics at the Terascale,
School of Physics, The University of Melbourne, Victoria 3010, Australia*

²*Institute for Particle Physics Phenomenology, Department of Physics,
Durham University, DH1 3LE, United Kingdom*

Simplified models provide an avenue for characterising and exploring New Physics for large classes of UV theories. In this article we study the ability of the LHC to probe the spin and parity quantum numbers of a new light resonance X which couples predominantly to the third generation quarks in a variety of simplified models through the $t\bar{t}X$ channel. After evaluating the LHC discovery potential for X , we suggest several kinematic variables sensitive to the spin and CP properties of the new resonance. We show how an analysis exploiting differential distributions in the semi-leptonic channel can discriminate among various possibilities. We find that the potential to discriminate a scalar from a pseudoscalar or (axial) vector to be particularly promising.

I. INTRODUCTION

After the discovery of the Higgs boson [1, 2], the particle physics community is eagerly expecting and awaiting the discovery of Beyond-the-Standard-Model (BSM) physics at the Large Hadron Collider. While the majority of attention from phenomenologists has been focussed on the possibility of heavy new particles at the high energy frontier, it could also be the case that light resonances have escaped notice from previous colliders such as LEP and the Tevatron, and may be discovered in the large datasets which the LHC will accrue in coming years.

This has been an area of particular interest due to the Galactic Centre excess of diffuse gamma-rays [3–6], which may be explained by dark matter (DM) annihilating via a light mediator into Standard Model (SM) particles [5, 7, 8]. In these cases the excess can be explained with scalar [9–12], pseudoscalar [13], or axial (or mixed coupling) vector mediators [14, 15]. The collider sensitivity to these mediators have been explored in a series of papers under the assumption that the mediator couples to the quarks and DM [16–23]. Since some analyses of the GC excess suggest that DM annihilation into b quarks provides a particularly good fit, some studies have assumed the mediator predominantly couples to the third generation quarks. In that case an important collider signal is associated production with a pair of top or bottom quarks [24–26], particularly for spin-1 mediators where LHC production via gluon fusion is forbidden by the Landau-Yang theorem [27, 28]. There has also been model building interest recently in top-philic Z' bosons in the context of a slight excess in $t\bar{t}h$ searches for SM Higgs boson production [29]. Some recent work has studied searches for $t\bar{t}$ resonances in the context of two Higgs doublet models [30–32], and on searches for top-philic dark matter mediators [33]. However, these works focus on the heavier resonances. It is therefore important to understand the ability of the LHC to discover and measure the properties of light new resonances with strong couplings to the third generation.

If such a new light (i.e. $m_X \lesssim 100$ GeV) resonance X is discovered in Run 2 of the LHC, a first priority will be the characterisation of its quantum numbers. In the context of resonances with strong coupling to top quarks studies have already been made in $t\bar{t}X$ production [26, 34, 35], focussing on the semi- and di-leptonic top decay channels, where either one or both tops decay leptonically. In the case of di-leptonic top decays, it is known (building upon older work on spin-polarisation in $t\bar{t}$ production [36]) that the azimuthal angle between the leptons encodes much of the relevant CP information. Related work has focussed on dijet angular correlations in $pp \rightarrow jjX$ [37], as well as extending results to NLO accuracy [38, 39].

In this paper we seek to extend these previous works in a number of ways. We explore other angular variables which may be of use in pinning down the quantum numbers of top-philic resonances at the LHC. Where most other works have focussed on the di-leptonic final state (with some exceptions [26, 40]) we perform a detector-level analysis of the semi-leptonic final states. We find that although the SM backgrounds are challenging, this final state will indeed be useful in the discovery and characterisation of new light resonances.

The structure of our paper is as follows: in Sec. II we introduce and specify the simplified models which we will study, and in Sec. III we introduce at parton level a number of different kinematic distributions which exhibit some sensitivity to the quantum numbers of the new resonance, before in Sec. IV we perform a full analysis in the semi-leptonic final state of the LHC sensitivity, providing both estimated discovery reach and cross sections required for the LHC to be able to discriminate among different simplified models.

II. SIMPLIFIED MODELS

We study the phenomenology of a variety of simplified models [41] with a new neutral resonance which we assume to be an eigenstate of parity and charge conjuga-

tion. Its couplings are restricted to the third generation quarks (bottoms and tops) only. For a scalar resonance S and a pseudoscalar resonance A , we assume the following CP-conserving interaction Lagrangians:

$$\mathcal{L}_S = - \sum_{q=b,t} \frac{g_q y_q}{\sqrt{2}} S \bar{q} q, \quad (1)$$

$$\mathcal{L}_P = - \sum_{q=b,t} \frac{g_q y_q}{\sqrt{2}} A \bar{q} i \gamma_5 q, \quad (2)$$

where y_q is the SM Yukawa couplings. We also study a vector resonance Z'_V and an axial vector resonance Z'_A with interaction Lagrangians given by

$$\mathcal{L}_V = - \sum_{q=b,t} g_q Z'^{\mu}_V \bar{q} \gamma^{\mu} q, \quad (3)$$

$$\mathcal{L}_{AV} = - \sum_{q=b,t} g_q Z'^{\mu}_A \bar{q} \gamma^{\mu} \gamma_5 q. \quad (4)$$

In all these cases the decay width of the resonance is set to its natural width calculated from the theory parameters at tree level. We do not include any interactions between X and possible dark matter candidates, focussing on its interactions with the SM (equivalently, there may be a coupling between X and dark matter, but we study the parameter space where $m_X/2 > m_{\text{DM}}$). In the case that the resonance is lighter than $2m_t$ it must decay into a pair of b quarks with a branching ratio equal to one (neglecting three-body decays). While these Lagrangians will also lead to dimension-five interactions with gluons for the scalar and pseudoscalar (whose CP properties can be probed in dijet angular correlations for instance [42]), in this paper we exclusively focus on what can be gleaned from associated production with tops.

We have implemented these models in `FeynRules` [43] which allows us to generate simulated events at the LHC using `MadGraph` [44] via the `UFO` [45] format.

III. SPIN AND PARITY DISCRIMINATING VARIABLES

In Fig. 1 we show the behaviour of the cross-sections for the four simplified models as functions of the resonance mass m_X . As has been demonstrated before [26], for low masses (below around 100 GeV) the $t\bar{t}A$ production cross section is quite suppressed relative to that of $t\bar{t}S$, and is smaller by over an order of magnitude below 40 GeV. We also observe similar behaviour (although not as extreme) in the $t\bar{t}Z'_V$ versus $t\bar{t}Z'_A$ cross sections. The differences between the cross sections become smaller as m_X increases, and are all within a factor of two at $m_X = 200$ GeV.

To attempt to understand this we have calculated the helicity amplitudes for $t\bar{t}A$ and $t\bar{t}S$ production, using the Weyl-van-der-Waerden spinous formalism for the case of massive particles [46]. However, due to the complicated 3-body phase space for the processes we study it is difficult to leverage these analytic results into an analytic

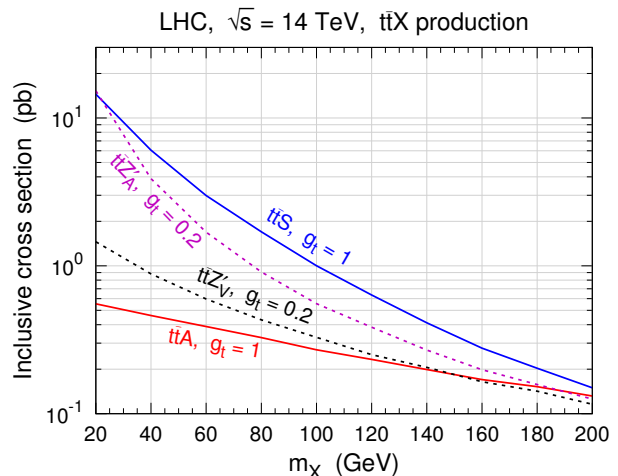


FIG. 1. This figure shows the $t\bar{t}X + \text{jets}$ ($X = S, A, Z'_V$, or Z'_A) production cross sections as functions of m_X at the 14 TeV LHC for the four simplified models.

understanding of the origin of the different cross-section values. As one might expect, the presence of the γ^5 appears to be responsible: comparing the scalar and pseudoscalar cases the γ^5 leads to sign change for a number of the helicity amplitudes, suggesting a destructive interference in the pseudoscalar scenario.

We now turn to the information available in the kinematic distributions which can be formed from the $t\bar{t}X$ final state ($X = S, A, Z'_V, Z'_A$), focussing on those which have particular sensitivity to the CP and spin properties. For clarity, we present our results in this section at parton level, before providing a full detector-level analysis in Section IV.

We show in Figs. 2(a) and 2(b) the distributions of the di-top invariant mass $m_{t\bar{t}}$ and the transverse momentum of the resonance $p_{T,X}$, for the four simplified models introduced above with the benchmark mass of $m_X = 50$ GeV. The distributions are normalised and hence independent of the coupling g_t , because we are primarily interested in the shape of the distributions rather than the precise values of the production cross sections. Both $m_{t\bar{t}}$ and $p_{T,X}$ (which are correlated) have previously been suggested as variables which may help distinguish between $t\bar{t}S$ and $t\bar{t}A$ production [34, 35, 40]; here we see that these variables are also sensitive to $t\bar{t}Z'_V$ and $t\bar{t}Z'_A$ production. The distributions are generally quite similar in shape. However, we notice that $t\bar{t}A$ leads to the hardest distributions, with a shift in the peak and a longer tail at large $m_{t\bar{t}}$ and $p_{T,X}$ compared to $t\bar{t}S$. $t\bar{t}Z'_V$ and $t\bar{t}Z'_A$ interpolate between these two behaviours: they lead to spectra which are harder than $t\bar{t}S$, but not so much as $t\bar{t}A$.

It is known that the azimuthal angle distribution between the two top quarks incorporates much information about the quantum numbers of the resonance X . Accessing this information is non-trivial however: the

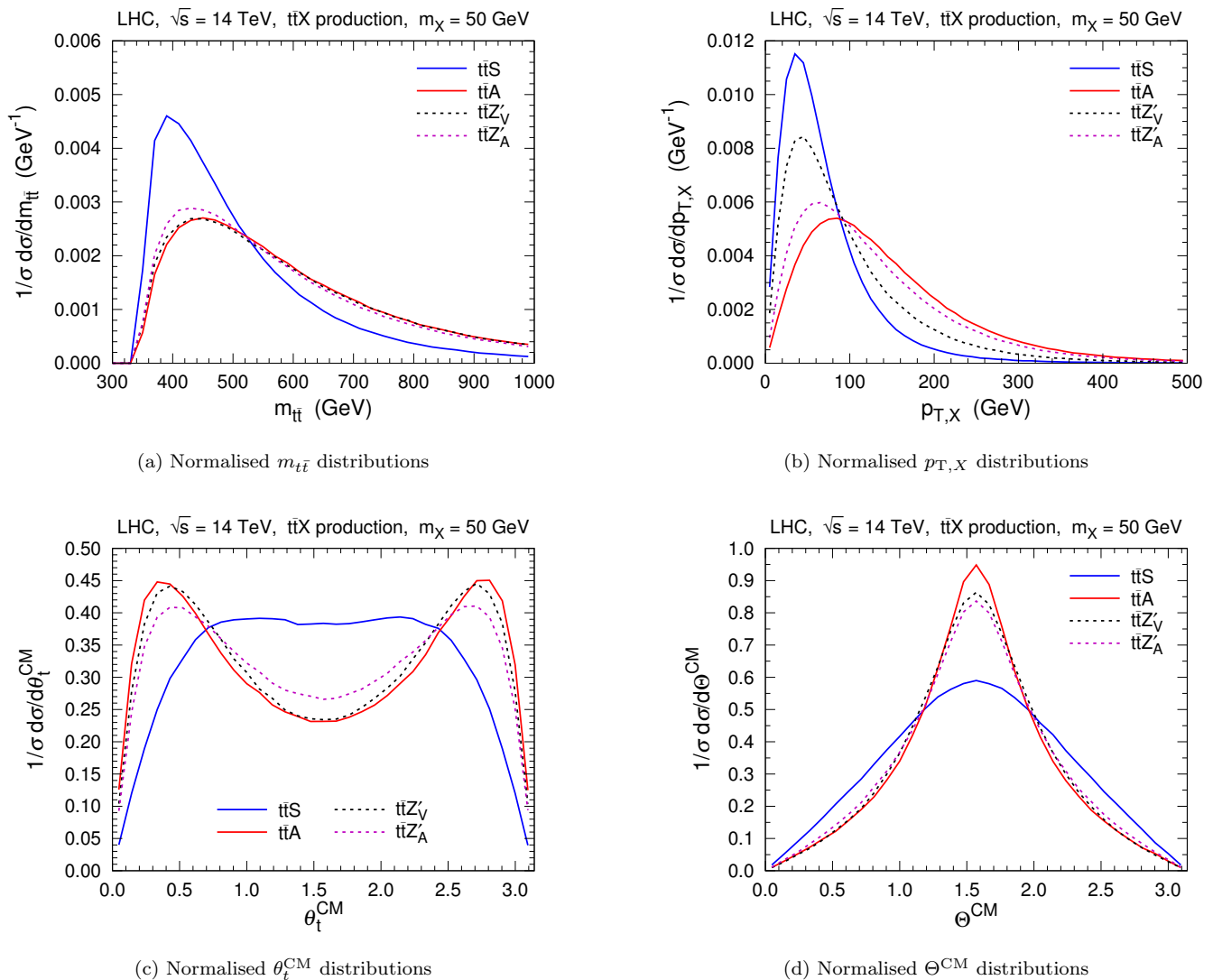


FIG. 2. This figure shows the normalised distributions of $m_{t\bar{t}}$ (a), $p_{T,X}$ (b), θ_t^{CM} (c) and Θ^{CM} (d) for parton-level $t\bar{t}X$ production with $\sqrt{s} = 14$ TeV and $m_X = 50$ GeV. Here $X = S, A, Z'_V,$ or Z'_A . The angular variables θ_t^{CM} and Θ^{CM} are defined in the CM frame of the $t\bar{t}X$ system. As shown in Fig. 3, θ_t^{CM} is the angle between t and the beamline, while Θ^{CM} is the angle between the normal vector to the $t\bar{t}X$ system and the beamline.

only case where the both tops could in principle be fully reconstructed without missing energy is the fully-hadronic scenario, which for any realistic analysis will be plagued by insurmountable QCD backgrounds. This has led Refs. [34, 35] (based on previous work on $t\bar{t}$ spin correlations [36, 47]) to explore the fully leptonic case, substituting the azimuthal angle between the leptons for the top quarks, an idea which has met with some success even when X decays to dark matter [35]. They have shown that constraints can be set on the top-quark Yukawa coupling in associated production towards the end of LHC Run 2 using these techniques.

We therefore consider other angular variables, derived from boosting to the centre-of-mass (CM) frame of the reconstructed $t\bar{t}X$ system. We have investigated a vari-

ety of different constructions, and present results for two of the most sensitive that we have found. As illustrated in Fig. 3, θ_t^{CM} is the angle between t and the beamline in the CM frame. The normalised θ_t^{CM} distributions are shown in Fig. 2(c). We find that this variable is particularly sensitive to $t\bar{t}S$ production, which exhibits a broad plateau at $\pi/2$. The other processes all have a double-peak structure, with $t\bar{t}A$ being the sharpest defined, and $t\bar{t}Z'_V$ and $t\bar{t}Z'_A$ (similar to $m_{t\bar{t}}$ and p_T above) interpolating between $t\bar{t}S$ and $t\bar{t}A$.

The other angular variable Θ^{CM} utilises the fact that in the CM frame the $t\bar{t}X$ system forms a plane. We consider the normal vector to this plane, and Θ^{CM} is angle between the normal and the beamline, as explained in Fig. 3. Fig. 2(d) shows the normalised Θ^{CM} distribu-

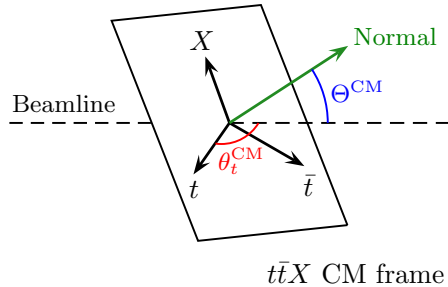


FIG. 3. This figure shows the definitions of θ_t^{CM} and Θ^{CM} in the CM frame of the $t\bar{t}X$ system. θ_t^{CM} is the angle between the t -quark and the beamline and Θ^{CM} is the angle between the normal vector to the $t\bar{t}X$ system and the beamline.

tions. The shape differences between the scalar and other resonances are not as great in this case, with the distributions for all the simplified models peaking at $\pi/2$. The $t\bar{t}S$ distribution is notable only in that it has the broadest distribution among them. While these variables show good sensitivity to the properties of the resonance X , a more realistic assessment of their utility requires a full analysis to be performed, which we now turn to.

IV. DETECTOR-LEVEL ANALYSIS

In this section we perform a detector-level LHC analysis for $\sqrt{s} = 14$ TeV incorporating the dominant backgrounds and reconstruction effects using the variables from the previous section to evaluate resonance properties. We focus on the challenging semi-leptonic final state where the hadronic top can be fully reconstructed, but where jet backgrounds are a larger problem than the dileptonic case. Ultimately, due to the small cross sections involved in $t\bar{t}X$ production, utilising both the semi-leptonic and leptonic final states will lead to a better understanding on the class of models we consider.

A. Event Simulation and Analysis Details

Previous work has demonstrated that the dominant background in $t\bar{t}X$ final states for low resonance masses comes from $t\bar{t}b\bar{b}$ production [26, 48]. While the $t\bar{t} +$ light jets rate is significant it is a subdominant background after b -tagging, but with similar kinematics to $t\bar{t}b\bar{b}$ and so will be suppressed by the same analysis cuts. We also include $t\bar{t}Z$ which is more subdominant, but important for a possible data-driven background estimation. We generate background and signal samples with MadGraph 5.2 [44] before showering them with PYTHIA 6 [49] and passing them through the Delphes 3 [50] detector simulation using the default ATLAS detector card. Thus, for jet $p_T = 100$ GeV,

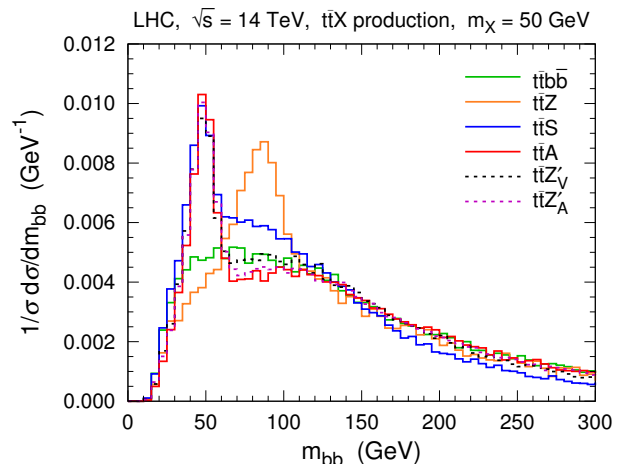


FIG. 4. This figure shows the normalised m_{bb} distributions after applying all the selection cuts except the cut on m_{bb} . For all the signals we take $m_X = 50$ GeV.

the b -tagging efficiency is assumed to be 73%, with the misidentification rates of c -jets and other light jets being 14% and 0.27%, respectively. Jets are clustered using the anti- k_T algorithm [51] with an angular distance parameter $R = 0.4$.

Selection cuts are adopted as follows. Firstly we require the selected events to contain exactly one charged lepton ℓ (electron or muon), exactly four b -tagged jets and at least two light jets. The lepton must be isolated from any jet via the condition $\Delta R > 0.4$. Moreover, the lepton and the jets should have $p_T > 25$ GeV and $|\eta| < 2.5$.

To reconstruct the hadronically decaying top we iterate through the reconstructed light jets and b -jets and find the combination which minimises

$$\chi^2 = \frac{(m_{jj} - m_W)^2}{m_W^2} + \frac{(m_{t,\text{had}} - m_t)^2}{m_t^2}, \quad (5)$$

where m_{jj} is the invariant mass of two light jets j_1 and j_2 , and $m_{t,\text{had}}$ is the invariant mass of j_1 , j_2 , and a b -jet b_1 . After that, to reconstruct the leptonically decaying top we iterate through the remaining b -jets and find the one b_2 which minimises

$$\chi^2 = \frac{(m_{t,\text{lep}} - m_t)^2}{m_t^2}, \quad (6)$$

where $m_{t,\text{lep}}$ is the invariant mass constructed by b_2 , the lepton, and the missing transverse momentum \mathbf{p}_T . The remaining b -jets b_3 and b_4 are used to search for the resonance X . We denote their invariant mass as m_{bb} and show the normalised distributions in Fig. 4 for our benchmark point with $m_X = 50$ GeV. There is a clear peak at the signal resonance position, and the $t\bar{t}b\bar{b}$ background is flat in the vicinity of the signal. As a reference for calibration, we also show the distribution of the $t\bar{t}Z$ background, which exhibits a clear Z peak. We observe that

TABLE I. Expected background and signal events per fb^{-1} after each step of the selection cuts for $m_X = 50$ GeV. We take $g_q = 1$ $t\bar{t}S$ and $t\bar{t}A$ signals, and $g_q = 0.2$ is assumed for the $t\bar{t}Z'_V$ and $t\bar{t}Z'_A$ signals.

	$t\bar{t}b\bar{b}$	$t\bar{t}S$	$t\bar{t}A$	$t\bar{t}Z'_V$	$t\bar{t}Z'_A$
No cut	24375	4211	428	714	241
1 lepton	4612	744	80.0	132	44.4
4 b -tags	106	33.9	5.15	7.12	27.5
≥ 2 light jets	72.9	22.1	3.51	4.86	18.7
$m_{jj} \in (60, 100)$ GeV	42.0	12.6	2.05	2.82	10.9
$m_{t,\text{had}} \in (120, 200)$ GeV	39.1	11.9	1.92	2.64	10.2
$m_{t,\text{lep}} \in (120, 220)$ GeV	30.2	9.87	1.52	2.09	8.07
$m_{bb} \in (35, 65)$ GeV	4.35	2.33	0.333	0.450	1.78

all signals exhibit long tails in the $b\bar{b}$ invariant mass, due to misattribution of the b 's from the tops and the b 's from the resonance. Based on experience with the SM Higgs, the use of boosted techniques should ameliorate this.

To further isolate the signal we impose the selection cuts $60 \text{ GeV} < m_{jj} < 100 \text{ GeV}$, $120 \text{ GeV} < m_{t,\text{had}} < 200 \text{ GeV}$, $120 \text{ GeV} < m_{t,\text{lep}} < 220 \text{ GeV}$, and $35 \text{ GeV} < m_{bb} < 65 \text{ GeV}$. The expected yields per inverse femtobarn for the $t\bar{t}b\bar{b}$ background and the signals after each step of selection cuts are presented in Table I. These cuts suppress the $t\bar{t}b\bar{b}$ background by a factor of $\sim 5 \times 10^3$. The $t\bar{t}Z$ background is lower than $t\bar{t}b\bar{b}$ by two orders of magnitude.

To estimate the expected exclusion on the signals we carry out a CL_s hypothesis test [52, 53] based on the m_{bb} distributions from 15 GeV to 200 GeV shown in Fig. 4. We scale up the $t\bar{t}b\bar{b}$ background by a factor of 1.2 in order to take into account the remaining backgrounds discussed earlier and assume a flat 10% systematic uncertainty on the total background. The expected 95% CL exclusion limits on the signal strength $\sigma(pp \rightarrow t\bar{t}X) \cdot \text{BR}(X \rightarrow b\bar{b})$ as functions of the integrated luminosity are shown in Fig. 5. These limits are comparable for the four simplified models due to the similarities in their production kinematics, and with the high-luminosity LHC it should be possible to bound the cross sections to the level of a few hundred femtobarns. For the pseudoscalar this corresponds to g_t just under 1 (*i.e.* essentially no suppression with respect to the SM Yukawa) while for the axial vector we can constrain g_t down to 0.08.

B. Expected Sensitivity for Discrimination among Simplified Models

Through the above reconstruction procedure, we can construct the 4-momenta of the hadronically decaying top, the leptonically decaying top, and the resonance X

from the identified jets and lepton:

$$p_{t,\text{had}} = p_{b_1} + p_{j_1} + p_{j_2}, \quad (7)$$

$$p_{t,\text{lep}} = p_{b_2} + p_\ell + \cancel{p}_T, \quad (8)$$

$$p_X = p_{b_3} + p_{b_4}. \quad (9)$$

The missing momentum \cancel{p}_T only contains transverse components and hence the reconstructed $p_{t,\text{lep}}$ is not as accurate as $p_{t,\text{had}}$. We can find a CM frame where $\mathbf{p}_{t,\text{had}} + \mathbf{p}_{t,\text{lep}} + \mathbf{p}_X = 0$. Therefore, these 4-momenta allow us to construct discriminating variables m_{tt} , $p_{T,X}$, $\theta_{t,\text{had}}^{\text{CM}}$, and Θ^{CM} that equivalent to the parton-level variables discussed in Sec. III. The normalised distributions for the signals and the $t\bar{t}b\bar{b}$ background with all the selection cuts applied are shown in Fig. 6. As expected, these detector-level variables catch the basic features of their parton-level counterparts demonstrated in Fig. 2. Note that $m_{tt} = (p_{t,\text{had}} + p_{t,\text{lep}})^2$ and $\theta_{t,\text{had}}^{\text{CM}}$ corresponds to the hadronically decaying top. An analogous variable $\theta_{t,\text{lep}}^{\text{CM}}$ can also be constructed from $p_{t,\text{lep}}$, but it is less powerful than $\theta_{t,\text{had}}^{\text{CM}}$ for discrimination among simplified models.

We perform a CL_s hypothesis test to investigate the discriminating power of each variables. Analogous to those in the ATLAS [54] and CMS [55] analyses for determining the spin and parity of the SM Higgs, the test statistic is defined as

$$Q = -2 \ln \frac{\mathcal{L}(s_2 + b)}{\mathcal{L}(s_1 + b)}, \quad (10)$$

where $\mathcal{L}(s + b)$ denotes the likelihood for the background b plus a signal hypothesis s . Thus, Q is used to discriminate between signal hypotheses s_1 and s_2 . For an observed value Q_{obs} , the exclusion of the hypothesis s_2 in favour of the hypothesis s_1 (denoted as “ s_1 vs s_2 ” below) is evaluated in terms of the modified confidence level

$$\text{CL}_s = \frac{P(Q \geq Q_{\text{obs}} | s_2 + b)}{P(Q \geq Q_{\text{obs}} | s_1 + b)}, \quad (11)$$

where $P(Q \geq Q_{\text{obs}} | s + b)$ is the probability for $Q \geq Q_{\text{obs}}$ under a hypothesis s .

Fig. 7 shows the expected 95% CL exclusion limits on the visible cross section σ_{vis} as functions of the integrated luminosity based on the discriminating variables, assuming 10% systematic uncertainty on the background. Here σ_{vis} is defined as the cross section taking into account the cut acceptance and efficiency. We assume each pair of signal hypotheses yield the same σ_{vis} , and evaluate the exclusion limit of one hypothesis in favour of the other one. In this way, the differences among these limits only come from the different behaviours of the signal hypotheses in the distributions shown in Fig. 6. Overall, the $p_{T,X}$ variable seems to be the most powerful one, except for the “ A vs Z'_A ” case, where the $\theta_{t,\text{had}}^{\text{CM}}$ variable is better than $p_{T,X}$ for a high integrated luminosity of $\sim 1 \text{ ab}^{-1}$. The $t\bar{t}S$ production is the easiest to be distinguished from the rest, because its distributions of all the discriminating variables behave most differently from others. The worst

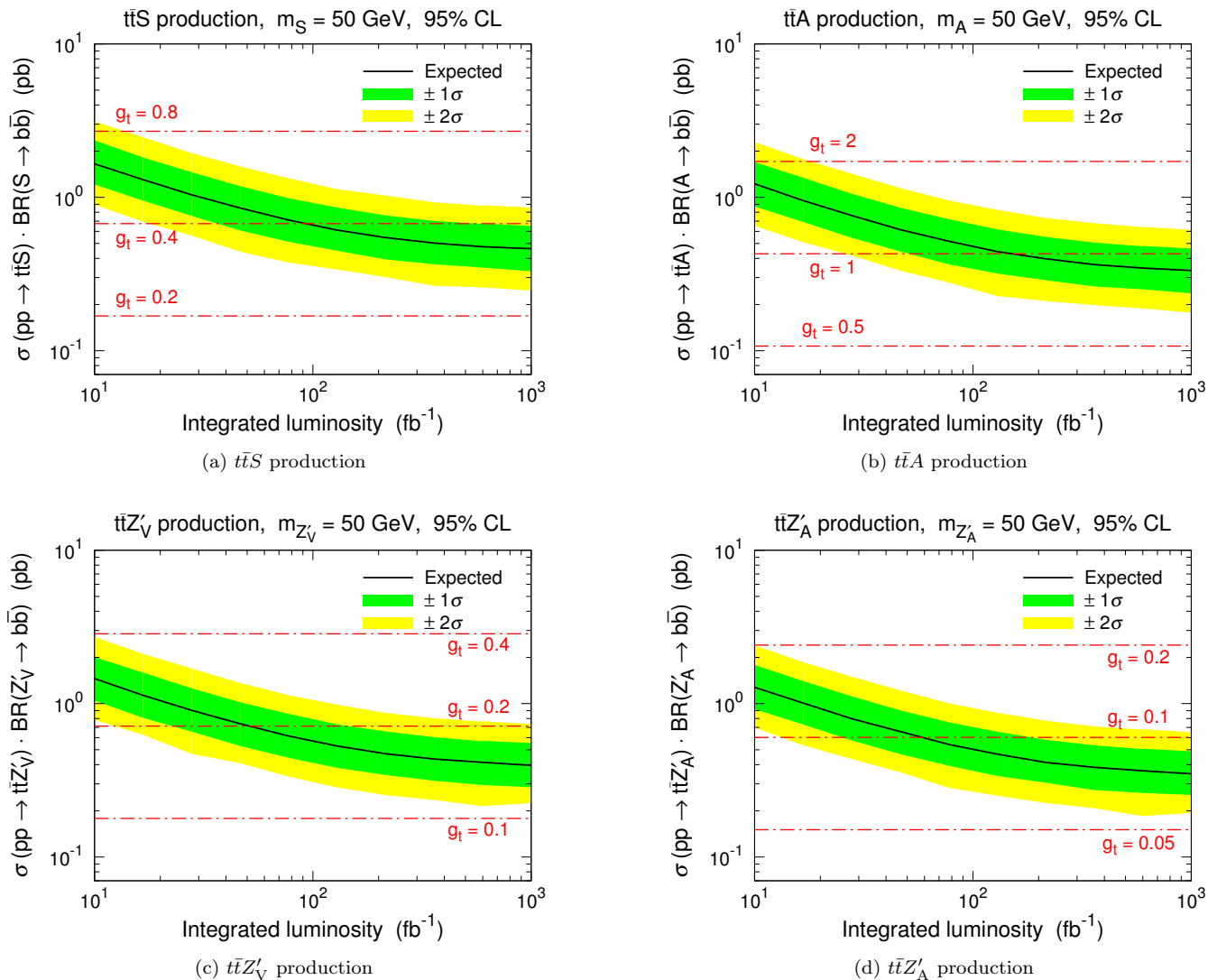


FIG. 5. This figure shows the expected 95% CL exclusion limits on the signal strength $\sigma(pp \rightarrow t\bar{t}X) \cdot \text{BR}(X \rightarrow b\bar{b})$ with $m_X = 50$ GeV as functions of the integrated luminosity at the 14 TeV LHC for $t\bar{t}S$ (a), $t\bar{t}A$ (b), $t\bar{t}Z'_V$ (c), and $t\bar{t}Z'_A$ (d) production. The dot-dashed lines denote the signal strengths for the g_t values labelled and $\text{BR}(X \rightarrow b\bar{b}) = 100\%$.

case is the discrimination between A and Z'_A , which yield similar shapes for every variable.

On the other hand, we also assume two signal hypotheses yield the same signal strength $\sigma(pp \rightarrow t\bar{t}X) \cdot \text{BR}(X \rightarrow b\bar{b})$ and estimate the corresponding exclusion limits. The results are presented in Fig. 8. In this case, the selection efficiency of the cuts affects the exclusion limits. From Table I, we know that the cut efficiencies for the $t\bar{t}S$, $t\bar{t}A$, $t\bar{t}Z'_V$, and $t\bar{t}Z'_A$ production are 5.5×10^{-4} , 7.8×10^{-4} , 6.3×10^{-4} , and 7.4×10^{-4} , respectively for $m_X = 50$ GeV. Due to the higher cut efficiencies for $t\bar{t}A$ and $t\bar{t}Z'_A$ production than that of $t\bar{t}Z'_V$ production, the exclusion limits for “ A vs Z'_V ” and “ Z'_V vs Z'_A ” are greatly improved, compared with those in Fig. 7. Given an integrated luminosity of 1 ab^{-1} and a signal strength of $\sim 1 - 2$ pb, we can discriminate between any pair of

simplified models at 95% CL except for the worst-case scenario of “ A vs Z'_A ”.

V. SUMMARY AND CONCLUSIONS

Searches for $t\bar{t}X$ production at the LHC are sensitive to a new resonance X coupled to the third generation quarks. If X is discovered, a further measurement of its parity and spin will be essential for revealing the underlying new physics. In this work we assumed a class of simplified models to describe the couplings between X and the third generation quarks, with X being a scalar, pseudoscalar, vector, or axial vector. Then we sought kinematic variables that are helpful for determining parity and spin quantum numbers and investigated the ex-

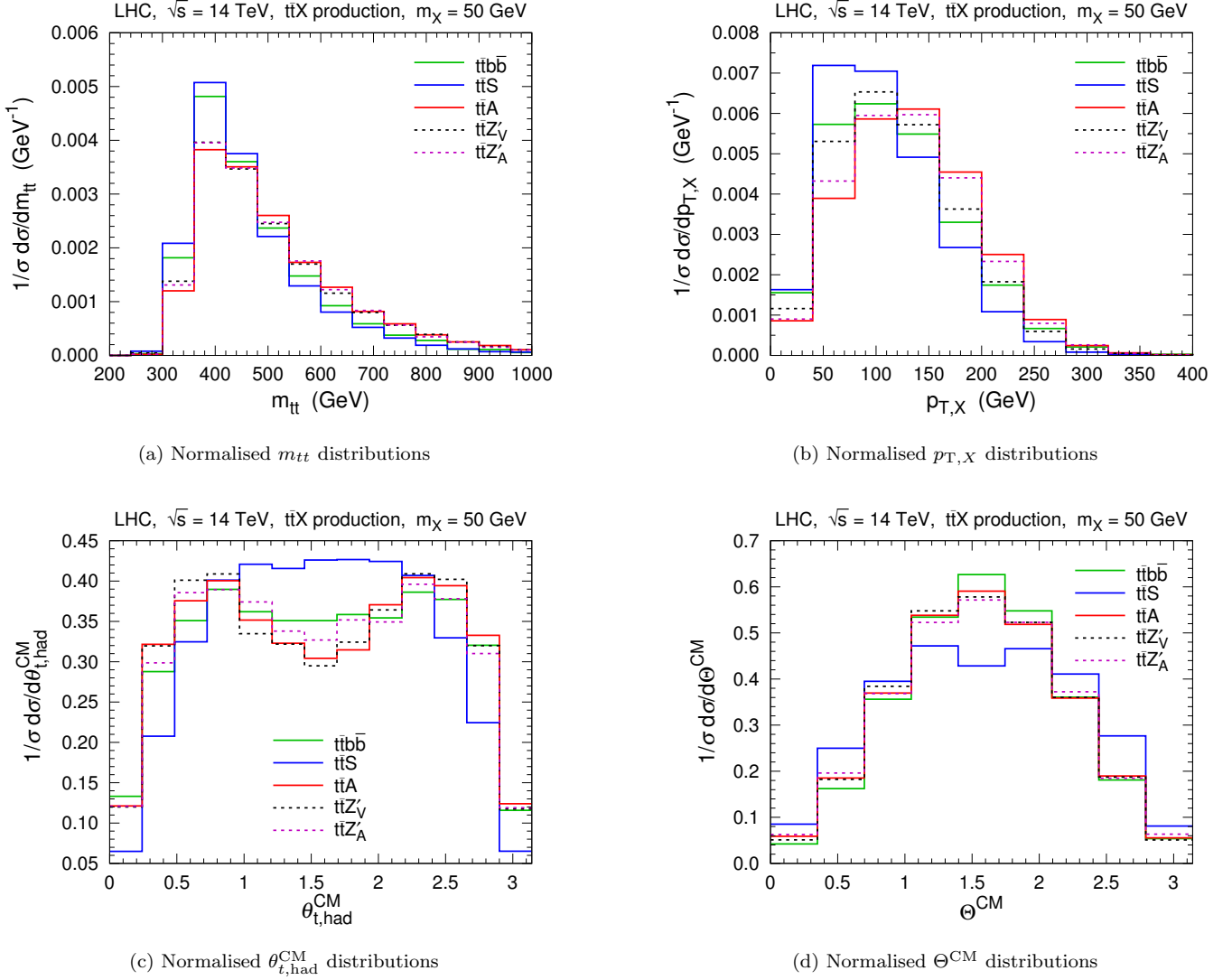


FIG. 6. This figure shows the normalised distributions of m_{tt} (a), $p_{T,X}$ (b), $\theta_{t,\text{had}}^{\text{CM}}$ (c), and Θ^{CM} (d) at detector level for the 14 TeV LHC and $m_X = 50$ GeV.

pected sensitivity through detailed simulation.

We have demonstrated four parton-level variables which exhibit different shapes for different models. Two of them are defined in the $t\bar{t}X$ CM frame. Therefore, using them requires a nearly full reconstruction of two tops and the resonance X , which can be achieved in the semi-leptonic channel. We have carried out the reconstruction procedure based on simulation in this channel and estimated the LHC sensitivity for discovery.

We constructed the detector-level counterparts of the parton-level variables and observed that their distributions preserve the important features for discrimination between the different simplified models. A CL_s hypothesis test has been performed to evaluate the sensitivity of discrimination separately based on each variables. We

found that the scalar is the easiest one to be distinguished from others while the hardest case is to discriminate between the pseudoscalar and the axial vector.

Further improvements to our analysis could be made by utilising jet substructure techniques to suppress the background more, and to allow a more accurate attribution of the b -jets used in the top and X reconstruction. It would also be interesting to perform a combined analysis of leptonic and semi-leptonic final states to see the ultimate sensitivity of the LHC. We leave this for future work.

Acknowledgements. MJD and ZHY are supported by the Australian Research Council. MS is supported in part by the European Commission through the ‘‘HiggsTools’’ Initial Training Network PITN-GA-2012-316704.

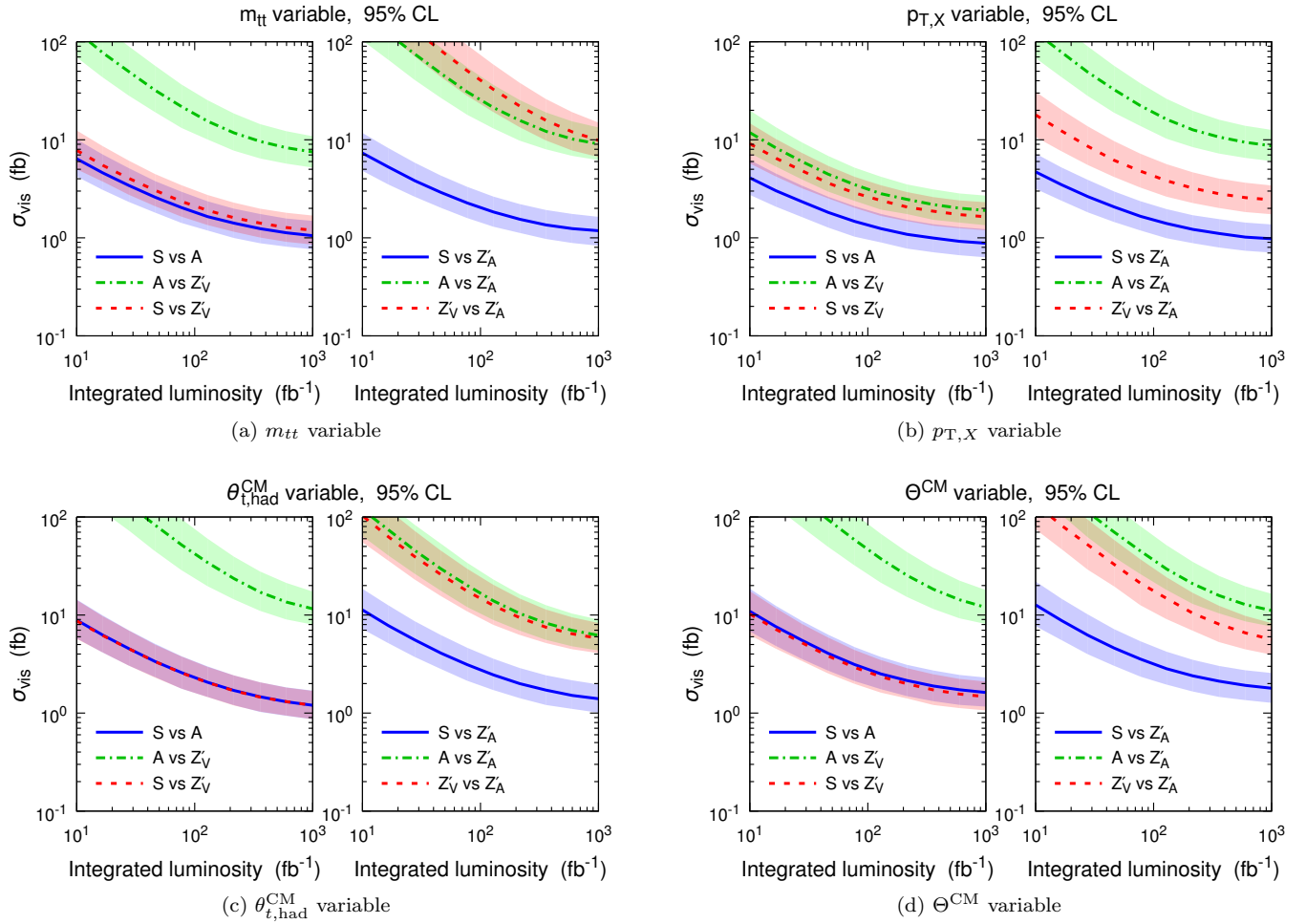


FIG. 7. This figure shows the expected 95% CL exclusion limits on the visible cross section σ_{vis} as functions of the integrated luminosity at the 14 TeV LHC based on the variables m_{tt} (a), $p_{T,X}$ (b), $\theta_{t,\text{had}}^{\text{CM}}$ (c), and Θ^{CM} (d). The lines denote the median value of the limit, while the coloured bands denote the $\pm 1\sigma$ range. “ s_1 vs s_2 ” corresponds to the exclusion of the signal hypothesis s_2 in favour of the signal hypothesis s_1 , assuming both hypotheses yield the same visible cross section.

-
- [1] G. Aad *et al.* (ATLAS), Phys. Lett. **B716**, 1 (2012), arXiv:1207.7214 [hep-ex].
- [2] S. Chatrchyan *et al.* (CMS), Phys. Lett. **B716**, 30 (2012), arXiv:1207.7235 [hep-ex].
- [3] D. Hooper and L. Goodenough, Phys. Lett. **B697**, 412 (2011), arXiv:1010.2752 [hep-ph].
- [4] C. Gordon and O. Macias, Phys. Rev. **D88**, 083521 (2013), [Erratum: Phys. Rev.D89,no.4,049901(2014)], arXiv:1306.5725 [astro-ph.HE].
- [5] T. Daylan, D. P. Finkbeiner, D. Hooper, T. Linden, S. K. N. Portillo, N. L. Rodd, and T. R. Slatyer, Phys. Dark Univ. **12**, 1 (2016), arXiv:1402.6703 [astro-ph.HE].
- [6] F. Calore, I. Cholis, and C. Weniger, JCAP **1503**, 038 (2015), arXiv:1409.0042 [astro-ph.CO].
- [7] P. Agrawal, B. Batell, P. J. Fox, and R. Harnik, JCAP **1505**, 011 (2015), arXiv:1411.2592 [hep-ph].
- [8] F. Calore, I. Cholis, C. McCabe, and C. Weniger, Phys. Rev. **D91**, 063003 (2015), arXiv:1411.4647 [hep-ph].
- [9] C. Boehm, M. J. Dolan, and C. McCabe, Phys. Rev. **D90**, 023531 (2014), arXiv:1404.4977 [hep-ph].
- [10] P. Ko, W.-I. Park, and Y. Tang, JCAP **1409**, 013 (2014), arXiv:1404.5257 [hep-ph].
- [11] M. Abdullah, A. DiFranzo, A. Rajaraman, T. M. P. Tait, P. Tanedo, and A. M. Wijangco, Phys. Rev. **D90**, 035004 (2014), arXiv:1404.6528 [hep-ph].
- [12] Z.-H. Yu, X.-J. Bi, Q.-S. Yan, and P.-F. Yin, Phys. Rev. **D91**, 035008 (2015), arXiv:1410.3347 [hep-ph].
- [13] C. Boehm, M. J. Dolan, C. McCabe, M. Spannowsky, and C. J. Wallace, JCAP **1405**, 009 (2014), arXiv:1401.6458 [hep-ph].
- [14] A. Berlin, D. Hooper, and S. D. McDermott, Phys. Rev. **D89**, 115022 (2014), arXiv:1404.0022 [hep-ph].
- [15] D. Hooper, Phys. Rev. **D91**, 035025 (2015), arXiv:1411.4079 [hep-ph].
- [16] O. Buchmueller, M. J. Dolan, and C. McCabe, JHEP **01**, 025 (2014), arXiv:1308.6799 [hep-ph].

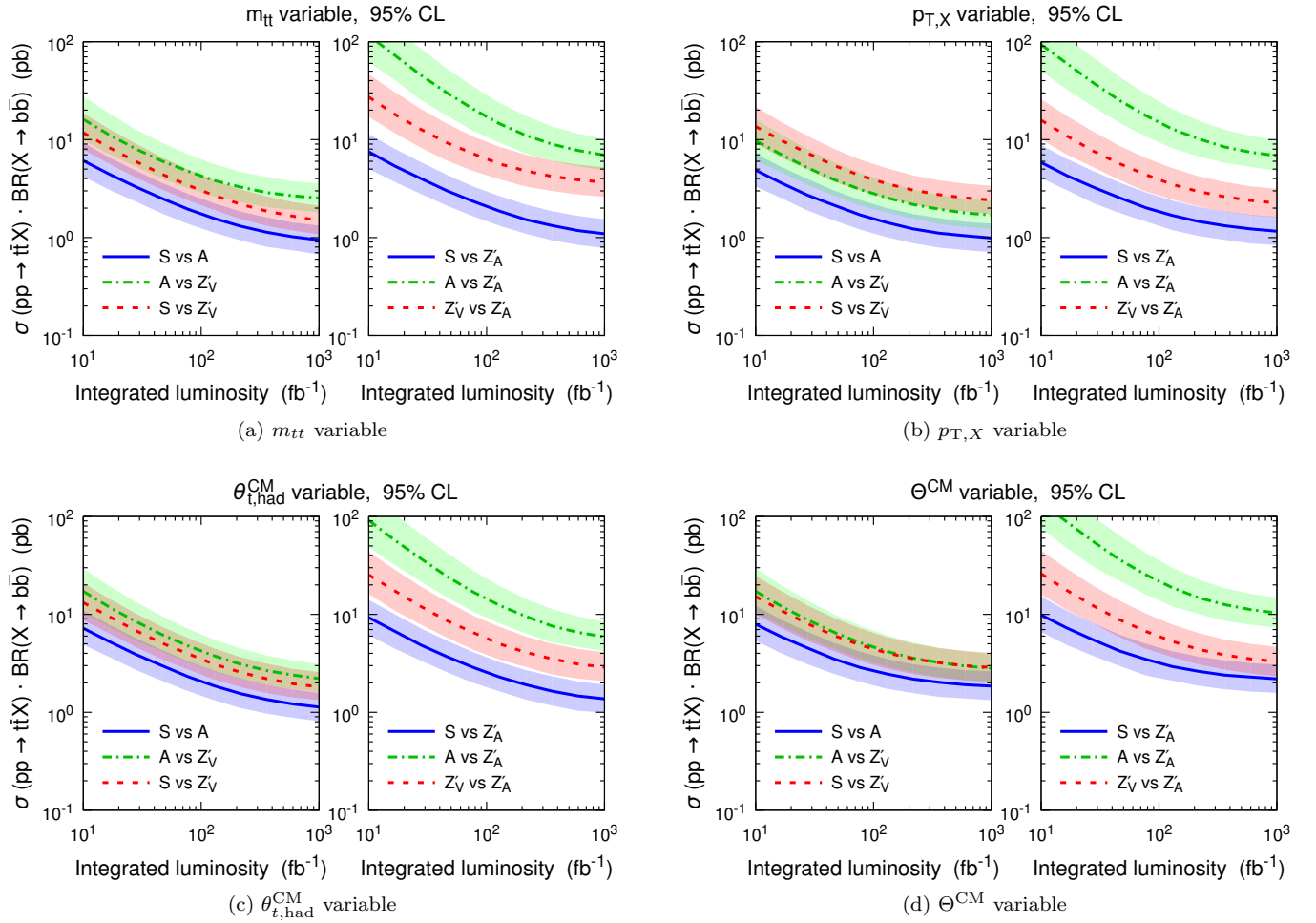


FIG. 8. This figure shows the expected 95% CL exclusion limits on the signal strength $\sigma(pp \rightarrow t\bar{t}X) \cdot \text{BR}(X \rightarrow b\bar{b})$ as functions of the integrated luminosity at the 14 TeV LHC based on the variables $m_{t\bar{t}}$ (a), $p_{T,X}$ (b), $\theta_{t,\text{had}}^{\text{CM}}$ (c), and Θ^{CM} (d). The lines denote the median value of the limit, while the coloured bands denote the $\pm 1\sigma$ range. “ s_1 vs s_2 ” corresponds to the exclusion of the signal hypothesis s_2 in favour of the signal hypothesis s_1 , assuming both hypotheses yield the same signal strength.

- [17] O. Buchmueller, M. J. Dolan, S. A. Malik, and C. McCabe, *JHEP* **01**, 037 (2015), arXiv:1407.8257 [hep-ph].
- [18] S. A. Malik *et al.*, *Phys. Dark Univ.* **9-10**, 51 (2015), arXiv:1409.4075 [hep-ex].
- [19] M. R. Buckley, D. Feld, and D. Goncalves, *Phys. Rev.* **D91**, 015017 (2015), arXiv:1410.6497 [hep-ph].
- [20] P. Harris, V. V. Khoze, M. Spannowsky, and C. Williams, *Phys. Rev.* **D91**, 055009 (2015), arXiv:1411.0535 [hep-ph].
- [21] Q.-F. Xiang, X.-J. Bi, P.-F. Yin, and Z.-H. Yu, *Phys. Rev.* **D91**, 095020 (2015), arXiv:1503.02931 [hep-ph].
- [22] U. Haisch and E. Re, *JHEP* **06**, 078 (2015), arXiv:1503.00691 [hep-ph].
- [23] G. Busoni *et al.*, (2016), arXiv:1603.04156 [hep-ex].
- [24] J. Kozaczuk and T. A. W. Martin, *JHEP* **04**, 046 (2015), arXiv:1501.07275 [hep-ph].
- [25] N. Craig, F. D’Eramo, P. Draper, S. Thomas, and H. Zhang, *JHEP* **06**, 137 (2015), arXiv:1504.04630 [hep-ph].
- [26] M. Casolino, T. Farooque, A. Juste, T. Liu, and M. Spannowsky, *Eur. Phys. J.* **C75**, 498 (2015), arXiv:1507.07004 [hep-ph].
- [27] L. D. Landau, *Dokl. Akad. Nauk Ser. Fiz.* **60**, 207 (1948).
- [28] C.-N. Yang, *Phys. Rev.* **77**, 242 (1950).
- [29] P. Cox, A. D. Medina, T. S. Ray, and A. Spray, (2015), arXiv:1512.00471 [hep-ph].
- [30] N. Chen, J. Li, and Y. Liu, *Phys. Rev.* **D93**, 095013 (2016), arXiv:1509.03848 [hep-ph].
- [31] S. Gori, I.-W. Kim, N. R. Shah, and K. M. Zurek, *Phys. Rev.* **D93**, 075038 (2016), arXiv:1602.02782 [hep-ph].
- [32] N. Craig, J. Hajer, Y.-Y. Li, T. Liu, and H. Zhang, (2016), arXiv:1605.08744 [hep-ph].
- [33] C. Arina *et al.*, (2016), arXiv:1605.09242 [hep-ph].
- [34] M. R. Buckley and D. Goncalves, *Phys. Rev. Lett.* **116**, 091801 (2016), arXiv:1507.07926 [hep-ph].
- [35] M. R. Buckley and D. Goncalves, *Phys. Rev.* **D93**, 034003 (2016), arXiv:1511.06451 [hep-ph].
- [36] G. Mahlon and S. J. Parke, *Phys. Rev.* **D53**, 4886 (1996), arXiv:hep-ph/9512264 [hep-ph].
- [37] U. Haisch, A. Hibbs, and E. Re, *Phys. Rev.* **D89**, 034009 (2014), arXiv:1311.7131 [hep-ph].
- [38] F. Demartin, F. Maltoni, K. Mawatari, B. Page,

- and M. Zaro, *Eur. Phys. J.* **C74**, 3065 (2014), arXiv:1407.5089 [hep-ph].
- [39] M. Backović, M. Krämer, F. Maltoni, A. Martini, K. Mawatari, and M. Pellen, *Eur. Phys. J.* **C75**, 482 (2015), arXiv:1508.05327 [hep-ph].
- [40] J. Ellis, D. S. Hwang, K. Sakurai, and M. Takeuchi, *JHEP* **04**, 004 (2014), arXiv:1312.5736 [hep-ph].
- [41] D. Alves (LHC New Physics Working Group), *J. Phys.* **G39**, 105005 (2012), arXiv:1105.2838 [hep-ph].
- [42] M. J. Dolan, P. Harris, M. Jankowiak, and M. Spannowsky, *Phys. Rev.* **D90**, 073008 (2014), arXiv:1406.3322 [hep-ph].
- [43] A. Alloul, N. D. Christensen, C. Degrande, C. Duhr, and B. Fuks, *Comput. Phys. Commun.* **185**, 2250 (2014), arXiv:1310.1921 [hep-ph].
- [44] J. Alwall, R. Frederix, S. Frixione, V. Hirschi, F. Maltoni, O. Mattelaer, H. S. Shao, T. Stelzer, P. Torrielli, and M. Zaro, *JHEP* **07**, 079 (2014), arXiv:1405.0301 [hep-ph].
- [45] C. Degrande, C. Duhr, B. Fuks, D. Grellscheid, O. Mattelaer, and T. Reiter, *Comput. Phys. Commun.* **183**, 1201 (2012), arXiv:1108.2040 [hep-ph].
- [46] S. Dittmaier, *Phys. Rev.* **D59**, 016007 (1998), arXiv:hep-ph/9805445 [hep-ph].
- [47] G. Mahlon and S. J. Parke, *Phys. Rev.* **D81**, 074024 (2010), arXiv:1001.3422 [hep-ph].
- [48] N. Moretti, P. Petrov, S. Pozzorini, and M. Spannowsky, *Phys. Rev.* **D93**, 014019 (2016), arXiv:1510.08468 [hep-ph].
- [49] T. Sjostrand, S. Mrenna, and P. Z. Skands, *JHEP* **05**, 026 (2006), arXiv:hep-ph/0603175 [hep-ph].
- [50] J. de Favereau, C. Delaere, P. Demin, A. Giammanco, V. Lemaitre, A. Mertens, and M. Selvaggi (DELPHES 3), *JHEP* **02**, 057 (2014), arXiv:1307.6346 [hep-ex].
- [51] M. Cacciari, G. P. Salam, and G. Soyez, *JHEP* **04**, 063 (2008), arXiv:0802.1189 [hep-ph].
- [52] T. Junk, *Nucl. Instrum. Meth.* **A434**, 435 (1999), arXiv:hep-ex/9902006 [hep-ex].
- [53] A. L. Read, *Advanced Statistical Techniques in Particle Physics. Proceedings, Conference, Durham, UK, March 18-22, 2002*, *J. Phys.* **G28**, 2693 (2002), [,11(2002)].
- [54] G. Aad *et al.* (ATLAS), *Proceedings, Meeting of the APS Division of Particles and Fields (DPF 2015)*, *Eur. Phys. J.* **C75**, 476 (2015), [Erratum: *Eur. Phys. J.* **C76**,no.3,152(2016)], arXiv:1506.05669 [hep-ex].
- [55] V. Khachatryan *et al.* (CMS), *Phys. Rev.* **D92**, 012004 (2015), arXiv:1411.3441 [hep-ex].